Author Postprint of the paper published in Supercond. Sci. Technol. 28 (2015) 035011

Magnetic shielding of an inhomogeneous magnetic field source by a bulk superconducting tube

K Hogan, J-F Fagnard, L Wéra, B Vanderheyden and P Vanderbemden

University of Liège, SUPRATECS research group, Department of Electrical Engineering & Computer science (B28), Sart-Tilman, B-4000 Liège, Belgium

E-mail: kevin.hogan@ulg.ac.be

Abstract. Bulk type-II irreversible superconductors can act as excellent passive magnetic shields, with a strong attenuation of low frequency magnetic fields. Up to now, the performances of superconducting magnetic shields have mainly been studied in a homogenous magnetic field, considering only immunity problems, *i.e.* when the field is applied outside the tube and the inner field should ideally be zero. In this paper, we aim to investigate experimentally and numerically the magnetic response of a high-Tc bulk superconducting hollow cylinder at 77 K in an emission problem, *i.e.* when subjected to the non-uniform magnetic field generated by a source coil placed inside the tube. A bespoke 3-D mapping system coupled with a 3-axis Hall probe is used to measure the magnetic flux density distribution outside the superconducting magnetic shield. A finite element model is developed to understand how the magnetic field penetrates into the superconductor and how the induced superconducting shielding currents flow inside the shield in the case where the emitting coil is placed coaxially inside the tube. The finite element modelling is found to be in excellent agreement with the experimental data. Results show that a concentration of the magnetic flux lines occurs between the emitting coil and the superconducting screen. This effect is observed both with the modelling and the experiment. In the case of a long tube, we show that the main features of the field penetration in the superconducting walls can be reproduced with a simple analytical 1D model. This model is used to estimate the maximum flux density of the emitting coil that can be shielded by the superconductor.

1. Introduction

Efficient magnetic screens are required in many applications involving high-sensitivity electric devices for which a low ambient magnetic field is necessary such as magneto-encephalography [1], SQUIDs [2], naval military applications [3], cryogenic current comparators [4], MRI [5] or cryogenic DC current transformers [6]. Most of these applications already require a cryogenic equipment so that the use of superconducting magnetic screens can be considered with negligible additional cost.

Bulk type II irreversible superconductors – and in particular high temperature superconductors (HTS) – can act as excellent passive magnetic shields over a large frequency range thank to their intrinsic flux pinning properties [7-9]. At low frequency, their efficiency has been shown to be superior to conventional solutions using ferromagnetic materials [7, 8]. Superconducting tapes made of Bi-2212/Bi-2223 [10] or MgB_2 [11] could also be considered to design magnetic screens. HTS materials can be used either at liquid nitrogen temperature, where shielding remains effective up to a few mT, or at lower temperatures (e.g. typically 10 K or lower), where shielding of magnetic inductions in excess of 1 tesla has been successfully demonstrated using hollow cylinders made of Bi-2212 [12] or MgB_2 [13].

In a passive superconducting shield, the magnetic field variations induce shielding supercurrents that flow in the superconducting walls and are able to oppose the applied field. In such a configuration the knowledge of the orientation (or the distribution) of the magnetic field is, *a priori*, not necessary, in contrast with active shields. Up to now, most studies on passive shields made of high temperature superconductor have been conducted in configurations where the applied magnetic field is external to the shield and homogeneous [6-9,12-22]. Consequently, only immunity problems have been investigated, *i.e.* the internal volume of the enclosure is protected from an external field. In such situations, the analysis of the magnetic response of the superconductor is simplified because one can easily identify a threshold value for the uniform external field, B_{lim}, above which the shield is penetrated. This threshold value can be used as a figure of merit of the shield. By contrast, with a non-homogenous source, the field penetration is not uniform and depends on both the source and the shield geometry [23]. The identification of a proper figure of merit is not straight forward. It should be emphasized that non-homogeneous or asymmetric configurations are relevant to many practical applications, e.g. shielding

the stray field of an electromagnet or of a dipole coil. The understanding of the magnetic response of superconducting materials in such situations is of great interest in view of designing efficient magnetic

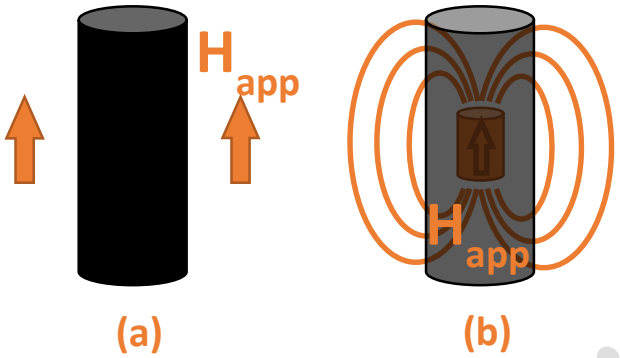

Figure 1. Schematic illustration of a tubular magnetic shield in (a) an immunity and (b) an emission configurations. In configuration (a) the applied field $\mathbf{H}_{app}$ is applied externally and strongly reduced in the internal volume. In configuration (b), the applied field $\mathbf{H}_{app}$ is generated by a coil or a permanent magnet and strongly reduced outside the tube.

shielding systems, levitation systems [23] or magnetic cloaking systems [24].

In this paper, we aim to investigate experimentally and numerically the magnetic response of a bulk, high temperature superconducting hollow cylinder subjected to the magnetic field generated by a small source coil placed inside the tube. This situation corresponds to an emission problem, *i.e.* the magnetic field generated by a magnetic source is confined in an enclosure to avoid any effect on sensitive equipment placed outside (see figure 1(b)). As a consequence the magnetic field to be shielded is intrinsically non-homogeneous. The purpose of the present work is to clarify the magnetic response of the material in this configuration.

This paper is organized as follows. Section 2 describes the experimental system used to carry out the magnetic shielding measurements. In section 3, the finite element model employed and the modelling hypotheses are detailed. The results of the measurements and of the modelling are presented in section 4. A comparison between experimental and numerical results is conducted in section 5. In section 6, we summarize the results and provide concluding remarks.

2. Experimental setup

The sample studied in this work is a hollow cylinder made of polycrystalline $Bi_{1.8}Pb_{0.26}Sr_2Ca_2Cu_3O_{10+x}$ (Bi-2223) from CAN Superconductors [25]. This tube is a non-textured polycrystalline ceramic manufactured by pressing powder. To excellent approximation, its properties are therefore assumed to be isotropic at the macroscopic scale. The geometrical characteristics of the cylinder are given in Table 1.

Table 1. Geometrical characteristics of the Bi-2223 hollow cylinder

Height (mm)	h = 80
Inner radius (mm)	r_{int} = 10.5
Wall thickness	e = 1.6

The magnetic field dependence of the sample critical current density $J_c(\mathbf{B})$ was determined experimentally using transport measurements on an open ring of 2 mm x 1.6 mm cross-section cut out from the sample. Kim's law [26] $J_c(\mathbf{B}) = J_{c0}\left(1+|\mathbf{B}|/B_1\right)^{-1}$ is used to describe this dependence with the two fitting parameters J_{c0} = 6.25 MA/m^2 and B_1 = 8.9 mT. The magnetic shielding properties of the cylinder were also determined under a homogeneous applied field: the maximal magnetic flux density (B_{lim}) that can be shielded at 77 K in axial configuration is $B_{lim} \approx 8$ mT when the sweep rate of the applied field $\mu_0 dH_{app}/dt$ is 1 mT/s. The critical exponent characteristic of the **E**-**J** law [27] $\mathbf{E}(\mathbf{J}) = E_c\left(|\mathbf{J}|/J_c\right)^n \mathbf{J}/|\mathbf{J}|$ was determined to be $n \approx 30$ at 77 K. It was obtained by sweep-creep measurements [28] which consist in observing the influence of the sweep rate of the applied magnetic field $\mu_0 dH_{app}/dt$ on B_{lim} when the sample is subjected to a homogenous magnetic field.

Table 2. Geometrical characteristics of the emitting coil

Number of turns	N = 989
Height (mm)	l = 14 mm
External radius (mm)	r_{ext} = 7 mm
Thickness (mm)	d = 6 mm

In the present work, all experiments are carried out in a liquid nitrogen bath (77 K) in zero field cooled conditions. The magnetic source is a copper coil whose geometrical characteristics are detailed in Table

2. It is designed in such a way that it can be placed coaxially as well as transversely (*i.e.* the axis of the tube and that of the coil are mutually perpendicular) inside the tube. The coil characteristics are chosen in such a way the largest possible magnetic field can be generated taking into the geometrical constraints, *i.e.* the coil is confined inside a sphere of diameter equal to the inner diameter of the superconducting cylinder. The maximum magnetic field that can be generated in the centre of the coil is 105 mT, corresponding to a drive current of 1.5 A. The coil is fed by a Delta SM70-22 DC power supply used in current-controlled mode.

The magnetic field is measured using two different Hall probes. First, a cryogenic high-sensitivity 3-axis Hall probe (Arepoc 3X-H) is fixed to a 3-axis XYZ micropositioning system consisting of 3 Thorlabs MTS50-Z8 (MTS50/M-Z8) motorized translation stages. This system allows one to carry out planar and circular (*i.e.* at constant distance from the external surface of the tube) mappings of the magnetic field. Second, several Lakeshore HGT-1001 miniature Hall probes are used to perform local measurements at locations that are inaccessible using the XYZ mapping system, e.g. inside the superconducting tube. All signals are recorded by a National Instrument Data Acquisition Card NI USB-6281. The DC power supply, the three motors and the acquisition card are controlled by a PC running LabView®.

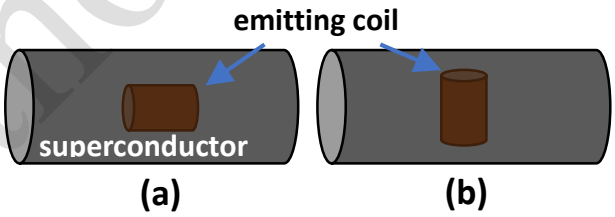

Figure 2. Schematic illustration on the two experimental configurations investigated in this work: (a) axial configuration (b) transverse configuration.

Two configurations were investigated experimentally (figure 2). The axial configuration consists of the emitting coil placed at the center of the superconducting cylinder and coaxially to the latter. The transverse configuration consists of the coil at the center of the cylinder and placed transversely.

3. Modelling

The numerical model that has been developed covers axisymmetrical configurations, which is the case when a source coil is placed coaxially to a superconducting tube (figure 2(a)).

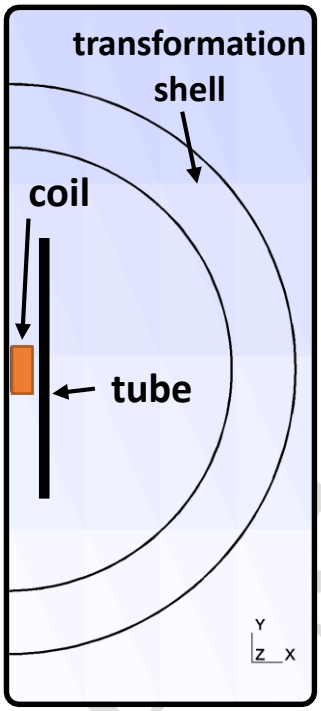

Figure 3. Geometry used for the finite element modelling

In general, the direction of the induced supercurrents inside the superconductor is *a priori* unknown. Indeed, in asymmetrical situations the current density is not necessarily perpendicular to the magnetic flux density, causing the appearance of longitudinal currents for which usual constitutive laws do not stand anymore and unusual critical states have to be considered [29-32]. By considering only axisymmetric situations, this problem does not arise because the direction of the supercurrents is imposed by the geometry; *i.e.* azimuthal in the present case. The situation analysed in this work is therefore reduced to a two dimensional problem.

A finite element method with an $\mathbf{A}-\phi$ formulation has been used to model the distribution of flux density and induced currents in axial configurations. The magnetic field and the electric field expressed in terms of $\mathbf{A}$ and ϕ are

$$\mathbf{B}=\nabla\times\mathbf{A}\,(1),$$

$$\mathbf{E}=-\frac{\partial\mathbf{A}}{\partial t}-\nabla\phi\,(2).$$

The geometry studied in the present work is shown on figure 3. The vector potential **A** is exclusively azimuthal, *i.e.* perpendicular to the modelling plane, given the geometry. The superconducting properties are modelled using the **E-J** power law

$$\mathbf{E} = E_c \left(\frac{|\mathbf{J}|}{J_c(\mathbf{B})} \right)^n \frac{\mathbf{J}}{|\mathbf{J}|} \quad (3)$$

and Kim law

$$J_c(\mathbf{B}) = J_{c0} \left(1 + \frac{|\mathbf{B}|}{B_1} \right)^{-1} \quad (4)$$

which considers the field dependence of the critical current Jc. Injecting Eqs. (1) to (4) in Maxwell equations, one obtains

$$\nabla \times \left(\mu^{-1} \nabla \times \mathbf{A} \right) = -\sigma \left(-\frac{\partial \mathbf{A}}{\partial t} - \nabla \phi, \nabla \times \mathbf{A} \right) \left(\frac{\partial \mathbf{A}}{\partial t} + \nabla \phi \right) + \mathbf{J_s} \quad (5)$$

where

$$\sigma(\mathbf{E}, \mathbf{B}) = \frac{J_c(\mathbf{B})}{E_c} \left(\frac{|\mathbf{E}|}{E_c} \right)^{\frac{1-n}{n}} \quad (6)$$

is the power law conductivity, and $\mathbf{J_s}$ is the current density that flows inside the source coil. One can observe that if $\mathbf{E} = \mathbf{0}$, the conductivity tends to infinity. In practical, a small quantity is added to the electric field in the expression of the conductivity to avoid numerical oscillations in the distribution of $\mathbf{E}$. To complete this model, we need to impose Dirichlet boundary conditions:

$$\mathbf{A} = \mathbf{0} \text{ and } \phi = 0$$

on the outer boundary using a jacobian transformation that sends the outer surface of the domain to infinity [33].

The mesh inside the superconductor is composed of quadrangles whose height (along the tube axis) is fixed and thickness changes with the radius. Thus, the inner surface of the superconductor has a higher density of mesh element than the outer surface of the superconductor in order to characterize in detail the penetration at low magnetic field. For the air and the inductor, the mesh is composed of triangular

elements. For a superconducting tube of 1.6 mm thickness and 80 mm height, the mesh size is typically 0.001 x 0.16 mm near the inner surface and 0.16 x 0.16 mm near the outer surface, leading to roughly 25000 quadrangles in the superconducting volume. For the air and the emitting coil, the mesh is composed of triangular elements. The total number of mesh elements is 86592.

This problem was solved using GetDP, an open source solver which is developed by the Applied and Computational Electromagnetics research unit of the University of Liège. Descriptions and details of this solver can be found in ref. [34].

The dimensions of the emitting coil and of the superconductor used in the modelling correspond exactly to the dimensions used in the experiment. The modelling is used to give relevant information about the way the magnetic field distribution is shaped around the shield and about the supercurrents distribution inside the screen.

The applied magnetic field depends only on the current density imposed in the source coil. The latter can be modified easily to apply triangular, harmonic or quasi-DC signals. In this study, the applied field is first increased to a maximal value B_{max} at a constant sweep rate, then it is decreased to zero at the same rate. This procedure is also used in the experiment.

4. Results

In this section we describe the results obtained when the tube and the emitting coil are first axial (figure 2(a)) and then perpendicular (figure 2(b)). Two preliminary points need to be emphasized.

(i) At low fields, the magnetic field generated by the emitting coil is screened completely by the superconducting tube and the magnetic flux density outside the superconductor is zero, which corresponds to the genuine magnetic shielding behaviour. As the current in the emitting coil is increased, magnetic flux penetrates progressively in the walls of the tube and eventually leaks out, leading to a measurable signal outside the superconductor. Measurements reported in this section are carried out purposefully in this regime, *i.e.* when the local magnetic flux density exceeds the penetration field of the superconductor.

(ii) In a non-homogeneous magnetic field configuration, as reported here, some confusion may arise about the terminology "applied field", since the local magnetic field experienced by the superconductor varies locally and, furthermore, differs from the field that would exist without superconductor (or above T_c). In the present work, the term "applied field" will refer systematically to the field at the centre of the emitting coil; this field being almost independent of the magnetic response of the superconductor. It should be kept in mind, however, than the central field differs, *a priori*, from the local field experienced by the superconductor.

4.1. Axial configuration

In the axial configuration, we first compare the experimental and modelled distribution of magnetic flux density outside the tube. Then the numerical modelling is used to draw magnetic flux lines and determine the distribution of induced currents in the superconductor.

Circular mappings

Figures 4 and 5 show the magnetic flux outside the cylindrical shield in the axial configuration. The distribution is recorded when the miniature Hall probe is mapped along a cylindrical surface, *i.e.* at constant distance (3.5 mm) of the outer surface of the superconducting tube.

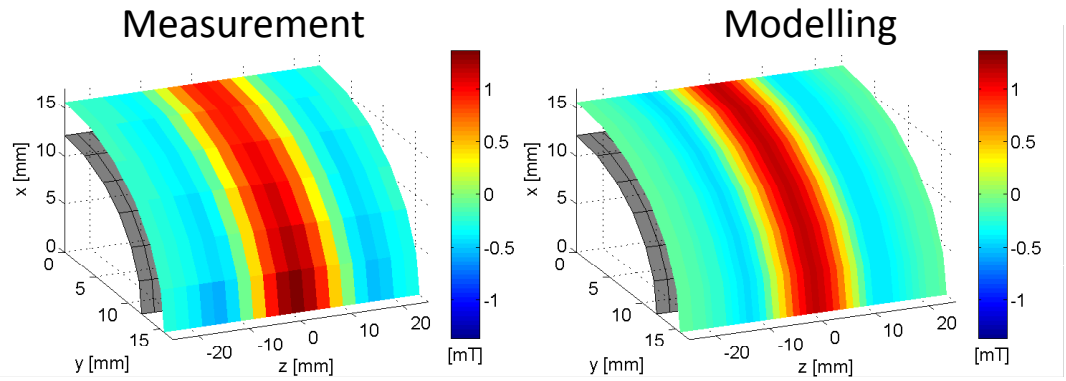

Figure 4. Circular mappings of the axial component of the measured/modelled magnetic field at 3.5 mm from the outer surface of the tube from an applied magnetic field of 87.5 mT

These measurements are carried out once the field has been ramped up, at a constant rate of 1 mT/s, to a magnetic induction in the centre of the coil of 87.5 mT and maintained at this value. The 3-axis Hall probe allows the axial (B_z) and radial (B_r) components of the local flux density to be determined, in

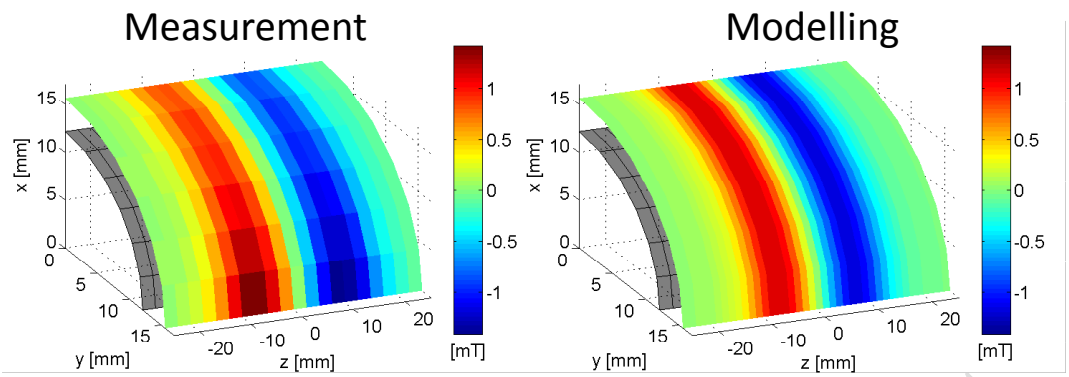

Figure 5. Circular mappings of the radial component of the measured/modelled magnetic field at 3.5 mm from the outer surface of the tube from an applied magnetic field of 87.5 mT

figures 4 and 5 respectively. In right-hand part of the figures, the flux distribution modelled using the procedure described in Section 3 is also shown. It should be emphasized that the superconducting parameters used for the modelling are those determined independently from previous experiments in uniform applied field (cf. Section 2).

First we examine the left hand parts of the figures (experimental data). As can be seen, the axial component B_z (figure 4) is maximum along the median plane of the tube, whereas the radial component B_r (figure 5) is nearly zero in the median plane and exhibits two extrema (positive, right and negative, left) located at $z = \pm 7$ mm, *i.e.* around the open ends of the emitting coil. One can also observe the expected axisymmetry of the measured magnetic flux density. Careful examination of figure 4 shows that this axisymmetry is not perfect; this phenomenon is due to the unavoidable uncertainty in positioning the emitting coil and will not be discussed further since it does not affect the main experimental features. The modelling results (right hand part) are in excellent agreement with the experimental results, both qualitatively and quantitatively. This observation is remarkable since modelling was carried out using superconducting parameters determined from independent experiments. As expected, modelled data are perfectly symmetric and emphasize the fact that the radial component (B_r) of the flux density leaking outside the tube is on the same order of magnitude as the axial component (B_z), although the geometrical configuration is axial. Qualitatively, the magnetic flux density distribution shown in figures 4 and 5 are close to the ones observed in the absence of the superconductor (not shown here). The spatial extension of magnetic flux, however, is slightly smaller with the superconductor, *i.e.* the minima and maxima are closer. This is due to the fact that only a finite axial portion of the magnetic

shield is penetrated totally. The larger the applied field, the larger the fully penetrated portion and thus the closer distribution to that without shield.

Magnetic field distribution

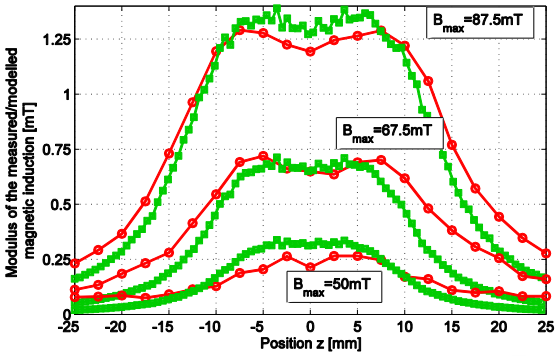

Figure 6. Modulus of the measured (red circle)/modelled (green square) magnetic flux density along the external surface of the superconducting shield at 3.5 mm for three different maximal applied fields (50, 67.5, 87.5 mT)). The sweep rate is 1 mT/s for the three situations.

Figure 6 shows the modulus of the measured and modelled magnetic flux density along the *z*-axis at 3.5 mm from the external surface of the cylinder. Three different maximal magnetic fields are applied (50 mT, 67.5 mT, 87.5 mT), using the same sweep rate (1 mT/s). The results plotted in this figure show the evolution of the magnetic distribution outside the shield once it is fully penetrated. The first location where the magnetic field reaches the outside is at $z = 0$ (median plane of the tube as well as of the emitting coil), as expected intuitively since this corresponds to the location where the magnetic shield is subjected to the highest applied field. As the applied magnetic fields increases, the portion of the superconducting shield that is fully penetrated increases, leading to the extension of the magnetic distribution outside the magnetic shield as observed in figure 6. The modelling results are in good agreement with the measurements. They point out that, once the flux leaks out the tube, the maximum modulus of magnetic flux density outside the tube is not located in the median plane ($z = 0$) but at two symmetric positions that spread apart on increasing the field.

In summary, the very good agreement between modelled and experimental curves, as evidenced from results plotted in figures 4, 5 and 6, validates the numerical modelling. This modelling was therefore

used to examine more carefully the complete distribution of flux lines as well as the distribution of induced currents in the tube, not directly accessible through experiments.

Magnetic flux density distribution

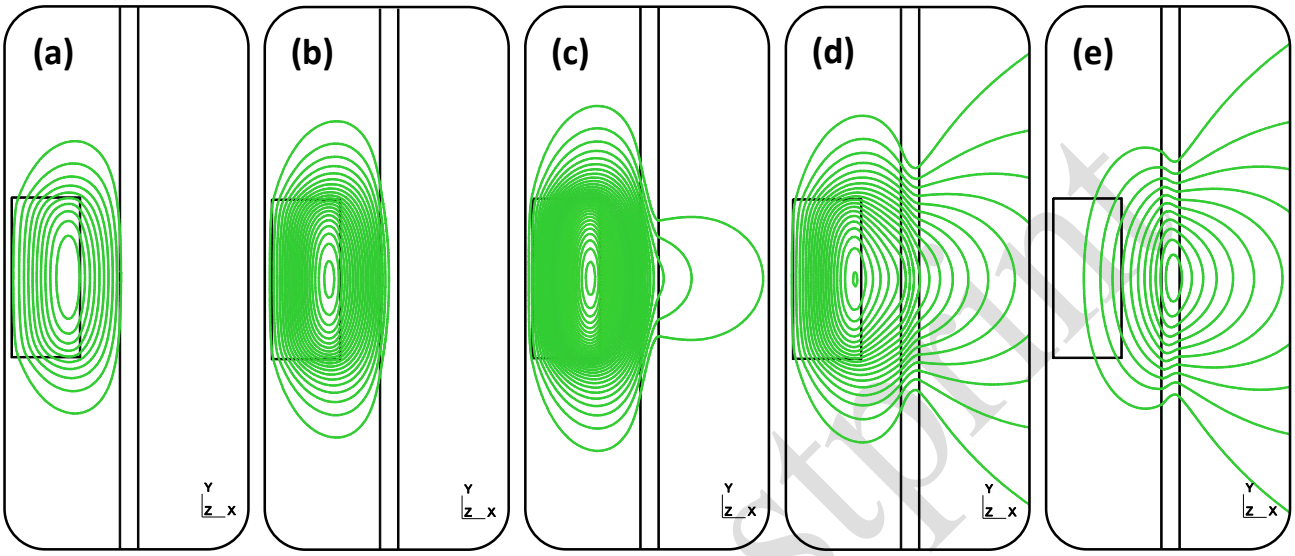

Figure 7. Magnetic flux distribution at five different time steps. The applied field is ramped up to 70mT at 1mT/s and ramped down to 0 at the same rate. Increase: (a) 22mT, (b) 43mT, (c) 64mT. Decrease: (d) 22mT, (e) 0mT). The last panel (e) shows the remnant magnetic flux distribution.

Figure 7 shows the modelling results of the evolution of the flux lines distribution at five different moments as the applied magnetic field is ramped up to 70 mT at a rate of 1 mT/s (figures 7(a) at 22 mT, 7(b) at 43 mT and 7(c) at 64 mT) and then down to 0 mT (figure 7(d) at 22 mT and 7(e) at 0 mT) at the same rate. In this figure, we plot contour lines of $\mathbf{r} \cdot \mathbf{A}$ which constitute a reasonable representation of the magnetic field lines [35]. The plots show the propagation of magnetic front inside the magnetic shield up to the moment when the magnetic field reaches the outside, *i.e.* when the local applied field exceeds the penetration field of the tube. Above that point (figures 7(c) and 7(d)), the modulus of the magnetic flux density outside the superconductor increases, as well as its spatial extension. As the applied magnetic field increases, the portion of the magnetic screen fully penetrated by flux lines grows. When the field reaches its maximum (70 mT in the present modelling), one can observe that the portion of the screen that is fully penetrated is roughly 1.5 times the height of the emitting coil. Figure 7(e) shows the remnant magnetic field that persists inside and outside the superconducting magnetic shield once the applied field is switched off. Another feature of interest, visible in the three panels on the left (7(a) to 7(c)) is a flux line concentration between the emitting coil and the inner wall of the cylinder.

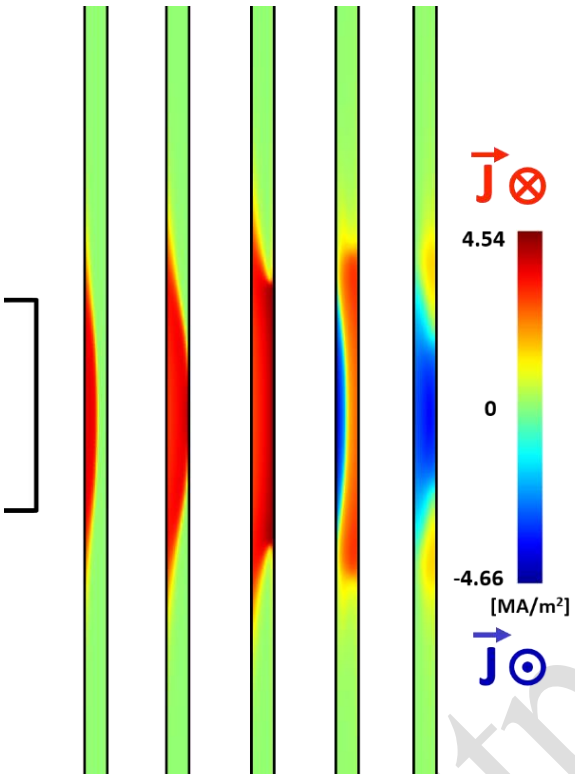

Figure 8. Current density distributions corresponding to the five time steps shown in figure 7. The applied field is ramped up to 70 mT at 1 mT/s and ramped down to 0 at the same rate.

This effect is due to the diamagnetic nature of the superconductor, which implies that the magnetic shield is subjected to a field higher than the one measured at the same point when there is no shield.

Figure 8 shows the azimuthal current distributions associated with each of the five flux line distributions shown in figure 7. Once again, one can clearly observe the magnetic flux front propagation. The portion of the superconductor where the supercurrents flow extents with the applied field and reaches about 1.5 times the height of the emitting coil when the applied field is maximum, as also observed for the flux line distributions. As soon as the applied magnetic field decreases and in the remnant state, there are persistent currents that flow in both direction generating a magnetic field outside and inside that are of opposite sign.

4.2. Transverse configuration

Now we turn to the transverse configuration investigated experimentally (2D numerical modelling could not be carried out due to the lack of symmetry). Circular mappings of the magnetic induction at 3.5 mm from the outer surface of the hollow cylinder were measured with and without the superconducting shield. Results are shown in figure 9. The three components of the magnetic field are expressed in a

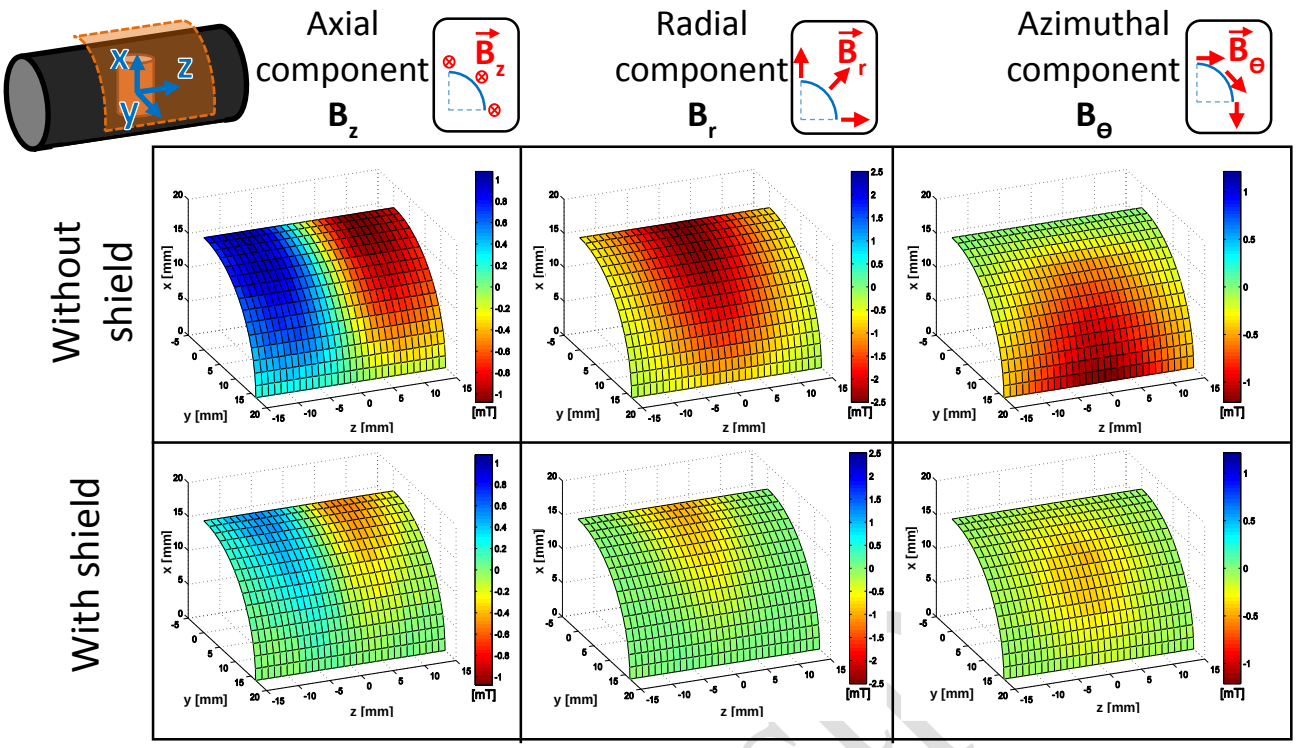

Figure 9. Circular mappings of the magnetic induction at 3.5 mm of the outer surface of the superconductor without (up) or with the superconducting shield (down). The three components are those of a cylindrical coordinate system associated with the hollow cylinder. The applied field is ramped up to 70 mT at 1 mT/s.

cylindrical coordinate system associated with the hollow cylinder. Without magnetic shield, the experimental spatial distribution of the three components B_z, B_r and B_θ displays the features that can be expected in this configuration: $B_z = 0$ in the median plane of the tube ($z = 0$), B_r is maximum $B_\theta = 0$ above the emitting coil. In comparing these results (upper part of figure 9) to the magnetic flux density leaking out the tube when it is superconducting (lower part of figure 9), one can observe that the distribution of the axial and radial components is not changed much. Their amplitude, however, are reduced with the magnetic screen. Concerning the azimuthal component B_θ, there is a clear change of distribution: without the shield, this component is maximum at lower centre of the mapping (as expected considering the field generated by the emitting coil) while with the shied, the amplitude is reduced and the maximum is now moved at the centre of the circular mapping. Given the magnetic field distribution in the presence of the shield, the supercurrents are expected to be flowing in the superconductor in a "saddle shape" just above the emitting coil.

5. Discussion

The experimental and modelled results above give important information on the magnetic flux density that can be measured outside the cylinder, *i.e.* the applied field is large enough so that magnetic screening is no longer effective. For practical purposes, however, it is of interest to have information about the maximum applied field B_p that can be screened efficiently. *In this section, we aim* at predicting this maximum field B_p and examining the magnetic flux density inside the cylinder in axial configuration when the magnetic screening is effective ($B < B_p$) or not ($B > B_p$), and to draw practical conclusions that can be applied to cylinders or emitting coils of other sizes. Then we use modelling to examine the influence of geometrical parameters of the cylinder (height and radius) on its magnetic shielding properties.

5.1 Analytical one dimension model

A simple one dimensional model has been developed to approximate the maximal applied magnetic field that can be screened by any tube B_p in axial configurations. We recall here that, according to definition given previously, the term "maximal applied field" corresponds to the field at the centre of the emitting coil before a magnetic field can be measured at the outer surface of the superconducting sample.

The model assumes an infinite superconducting hollow cylinder (internal radius r_1, external radius r_2) of constant critical current density J_c. The flux lines are assumed to be axial (*i.e.* directed along z direction) only. The model is based on the magnetic flux conservation in the plane $z = 0$ and assumes that all flux lines generated by the emitting coil (mean radius r_0) have three possible return paths:

(i) At low fields, no magnetic flux penetrates into the superconductor; return flux lines are therefore constrained in the empty space between the emitting coil and the wall of the tube (*perfect shielding* state).

(ii) At medium fields, magnetic flux penetrates partially in the wall of the cylinder; return flux lines are shared between the inner empty space and the wall of the tube (*partially penetrated* state).

(iii) At large fields, magnetic flux escapes from the cylinder; return flux lines are shared between the inner empty space, the wall of the tube and the free space outside the tube. This latter configuration is illustrated in figure 10 (*fully penetrated* state).

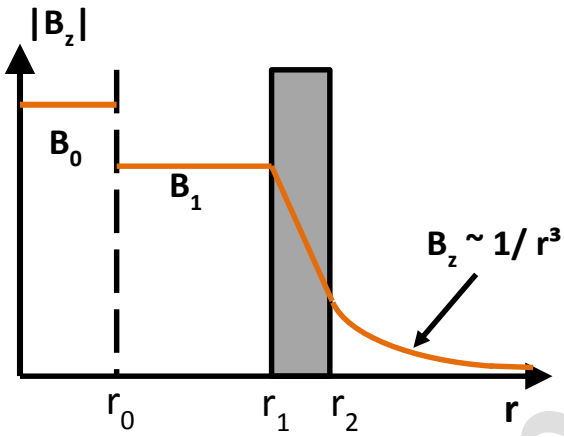

Figure 10. Illustration of the magnetic flux distribution for the analytical 1D model in the case of full penetration. r_0 is the mean radius of the emitting coil, r_1 and r_2 are respectively the inner and outer radii of the hollow cylinder.

The magnetic flux density is supposed uniform inside the emitting coil (B_0) and in the inner space between the coil and the inner surface of the superconductor (B_1). Inside the superconducting wall, the Bean model is used. Note that the model does not take into account reversible flux penetration due to Meissner currents (nor does the 2D model used previously). This is justified by the irregular shape of the polycrystalline material investigated (leading possibly to several local flux concentrations along the surface) as well as the fact that the lower critical field to consider is H_{c1j}, the lower critical field characteristic of grain boundaries (joints), which is often found to be much smaller than H_{c1g}, i.e. the lower critical field of the grains themselves; this means that a critical state model is often found to be appropriate for Bi-based ceramics at low fields [36,37]. This is also the case for magnetic shielding studies carried out in uniform field conditions [16]. Outside the tube, the flux density is supposed to decrease following a cubic power law $B \propto 1/r^3$. After calculations, one can obtain the following expressions for B_1 in terms of B_0:

$$B_1 = \frac{{r_0}^2}{{r_1}^2 - {r_0}^2} B_0 \quad (7)$$

$$\left(\frac{B_1}{\mu_0 J_c}\right)^3 + 3r_1\left(\frac{B_1}{\mu_0 J_c}\right)^2 + 3\left({r_1}^2 - {r_0}^2\right)\left(\frac{B_1}{\mu_0 J_c}\right) = 3{r_0}^2\left(\frac{B_0}{\mu_0 J_c}\right) \quad (8)$$

$$B_1 = \left(\frac{{r_0}^2}{{r_1}^2 + 2{r_2}^2 - {r_0}^2} \right) B_0 + \left(\frac{2\mu_0 J_c}{{r_1}^2 + 2{r_2}^2 - {r_0}^2} \right) \left(\frac{5}{6}{r_2}^3 - r_1{r_2}^3 + \frac{1}{2}{r_1}^2 r_2 - \frac{1}{3}{r_1}^3 \right) \quad (9)$$

respectively for the perfect shielding, partially and fully penetrated states. Note that strictly speaking, Eq. (8) does not give B_1 but corresponds to the cubic equation allowing B_1 to be numerically determined once numerical values for J_c and geometrical parameters are introduced. Using numerical parameters of the experiment described in the preceding sections, one can observe that the shield is subjected to a magnetic field larger than there would be without the shield. This magnetic flux concentration is due to the diamagnetic behaviour of the superconductor and depends primarily on the volume of the free space between the emitting coil and the tube. Consequently, this phenomenon - enhanced when the space between the coil and the screen is reduced - affects strongly the achievable compactness of the shield. In this simple model, the maximum applied magnetic field B_p corresponds to the transition between the partially and fully penetrated states, it is given analytically by

$$B_p = \frac{\mu_0 J_c}{3{r_0}^2} \left[\left({r_2}^3 - {r_1}^3 \right) - 3{r_0}^2 \left(r_2 - r_1 \right) \right] \quad (10)$$

Once the applied field is greater than that value, the magnetic induction B_1 increases linearly with B_0, as shown by Eq. (9).

It is instructive to compare the results obtained by this 1D model to those given by the 2D finite element modelling results and to experimental data. This is done in figures 11 and 12.

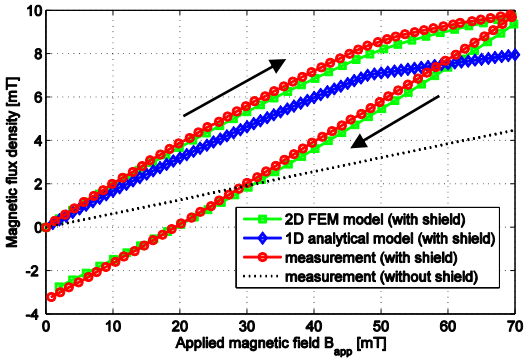

Figure 11. Axial magnetic flux density in the inner space between the coil and the wall of the superconductor at $z = 0$. The graph shows the experimental data (with or without magnetic shield), the theoretical prediction given by the analytical 1D model and the results of the 2D Finite Element Modelling (FEM). The sweep rate is 1 mT/s in all cases.

Figure 11 depicts the evolution of the magnetic flux density B_1 in the inner space between the coil and and tube as a function of the applied magnetic field, *i.e.* the field at the centre of the emitting coil. The applied field is swept from 0 to 70 mT at 1 mT/s and swept back to 0 at the same rate. Experimental data for B_1 are obtained using a miniature Hall probe. The numerical value of "constant J_c" required for the analytical 1D model (increasing branch only) is taken from the experimental Kim-like $J_c(\mathbf{B})$ by assuming that the magnetic field inside the super conductor when fully penetrated is roughly 7 mT. On figure 11, one can observe that the magnetic flux concentration occurs, *i.e.* that the values of B_1 for the increasing branch are substabtially larger than the flux density measured without superconductor (dotted black line). Further, the 2D finite element model is shown to be in excellent quantitative agreement with the measurements. The analytical 1D model clearly underestimates the inner magnetic field. This is due to the fact that the magnetic field is supposed homogeneous. However, the model gives a good results concerning the maximum magnetic field that can be applied by the emitting coil. Once the applied field is switched off, persistent currents in the wall of the tube give rise to a remnant magnetic flux which is density negative because it arises from the shielding currents flowing to oppose the variation of the decreasing applied magnetic field.

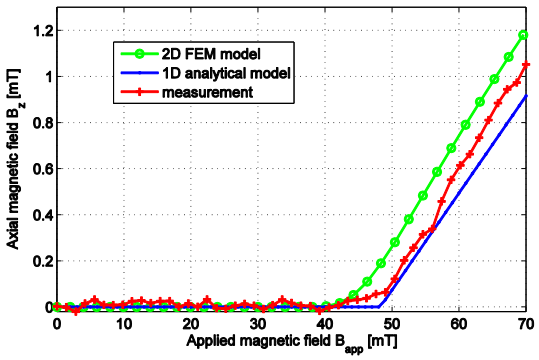

Figure 12. Axial magnetic field on the outer surface of the superconductor at z = 0: measurement, analytical 1D model and 2D Finite Element Modelling. The sweep rate is 1 mT/s.

Figure 12 shows the evolution of the axial magnetic flux density against the outer surface of the superconductor at 0.1 mm from the surface. The field at which the flux density merges from the noise level directly gives the full penetration field B_p, estimated here to be 45 mT. Both the finite element modelling and the analytical model are in good agreement with the measurement regarding this value.

The evolution of the measured flux density is not linear once full penetration is reached. This nonlinearity cannot be predicted by the analytical model because a field-independent J_c is assumed.

In summary, the above results obtained for axial configurations give us information about the flux density inside superconductor and allow one to determine the maximum flux density that can be shielded in these configurations. Remarkably, the approximate 1D analytical model gives results that are in excellent agreement with the more sophisticated 2D finite element model as well as with experimental data. Such agreement can be related to the fact that flux lines at the inner surface of the superconductor are mainly axial, as shown by results plotted in figures 7(a) to 7(c). This analytical model can thus be used to estimate at first order the magnetic performances of a superconducting magnetic screen of any internal and external radii (r_1 and r_2), subjected to the field produced by an emitting coil of radius r_0 placed axially.

5.2 Influence of the geometrical parameters of the superconducting sample

In this last section, the finite element model – compared to the analytical model - is used to investigate the influence of the geometry of the sample on the magnetic field distribution. The thickness of the hollow cylinder is kept constant and the two investigated parameters are the height and the inner radius of the tube. For every situation, the applied magnetic field is ramped up to 105 mT and ramped down to 0 mT at a rate of 1 mT/s.

(i) Effect of the height

We first consider the case of a tube of inner diameter of 21 mm which correspond to the dimension of the sample investigated experimentally. The sample is kept centered with the coil. Figure 13 shows the distribution of the magnetic flux density along the axial direction (z), at 1.9 mm from the external surface of the tube for several tube heights ranging from 10 mm to 80 mm. For the smallest tube investigated (h = 10 mm, blue circles), the two extrema of magnetic flux density are clearly located beyond the tube height (-5 mm < z < 5 mm), indicating that most of the the magnetic flux leaks out through the opening ends. For h = 20 mm (*i.e.* -10 mm < z < 10 mm, green squares), such two extrema outside the tube disappear but the leaking flux density is still important. For h = 30 mm, the extrema outside the tube

disappear completely and, remarkably, magnetic flux density profiles remain quite unchanged for longer tubes (h = 40 mm and 80 mm).

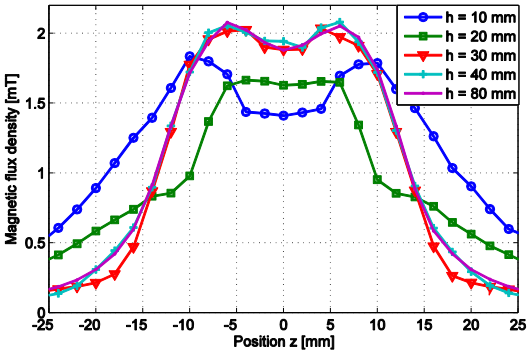

Figure 13. Modelled magnetic field distribution along the z-axis at 1.9 mm from the outer surface of the superconductor for an applied field of 105 mT.

As observed earlier in section 4, the shielding currents in the superconductor are located mainly in a portion of the screen whose height is roughly about 1.5 times that of the emitting coil. This is confirmed here by the above results; once the height is greater than 30 mm, the height has nearly no influence on the magnetic field distribution outside the screen. One can also observe that the magnetic field around z = 0 mm decreases when the height decreases from h = 40 mm. Beyond the extremities of the sample, however, the opposite situation is observed: the magnetic field increases. This is due to the flux lines that bypass the screen when its height is small compared to the one of the coil. This induces a decrease in the magnetic concentration effect between the emitting coil and the sample because the magnetic flux can extend around the screen.

(ii) Effect of the radius

Here we investigate the effect of increasing the inner radius of the superconducting hollow cylinder while keeping both the height and the wall thickness constant. Figure 14 and 15 show respectively, the magnetic flux density inside the shield at 1 mm from the inner surface and outside the shield at 1.4 mm from the outer surface. Four superconductors of different inner radii (11 mm, 13 mm, 15 mm and 17 mm) are investigated. Figure 14 shows that the magnetic concentration between the emitting coil and the shield decreases as the radius of the screen increases, as expected intuitively. Therefore, by increasing the radius of the shield, one can apply higher field before flux lines leak out of the magnetic shield. This is confirmed by the results shown in figure 15. On increasing the radius of the cylinder, the

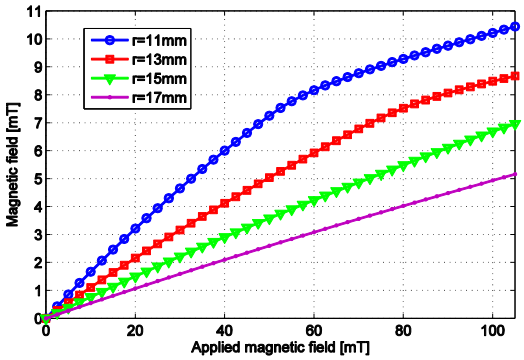

Figure 14. Evolution of the magnetic field when $z = 0$ at 1 mm from the inner surface of the superconducting shield for different radii as the applied magnetic field is ramped up to 105 mT at a rate of 1 mT/s

full penetration field B_p – corresponding to the applied field above which magnetic flux is detected outside the shield – increases. It should be noted, however, that this improvement of the maximum field that can be shielded occurs to the detriment of the magnetic flux density towards the ends of the cylinder, which is found to increase with increasing radius of the cylinder. The dotted lines in figure 15 show the theoretical predictions obtained with the analytical 1D model, giving a reasonable order of magnitude and being in qualitative agreement with the above observations.

When designing a magnetic shield intended to screen a given source coil or device, one wants usually to minimize its volume both for convenience of manufacturing and reduction of cost. The results obtained in the present work show that concentration of magnetic flux represents the main constraint on the reduction of the shield volume. If the radius of the shield is too small, the high value of the local field experienced by the superconductor will yield penetration through the walls. Therefore, there must be an optimal design for the magnetic shield in emission configuration.

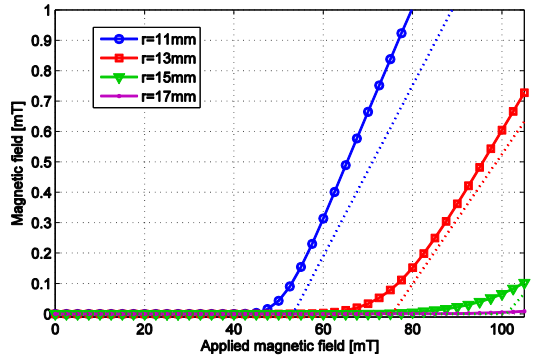

Figure 15. Evolution of the magnetic field at 1.4 mm from the outer surface of the superconducting shield for different radii as the applied magnetic field is ramped up to 105 mT at a rate of 1 mT/s. The dotted lines show the theoretical predictions obtained by the analytical 1D model.

6. Conclusion

The magnetic response of a bulk irreversible type-II superconducting tube subjected to an inhomogeneous magnetic field has been investigated both experimentally and numerically. We have considered the situation of an emission problem with an emitting source coil placed inside the magnetic shield. The centre of this coil coincides with that of the tube; the coil is either axial or transverse to the tube. Miniature flux mapping using a 3-axis Hall probe moved along a cylindrical surface (*i.e.* at constant distance from the outer wall of the tube) has proved to be an efficient tool to reveal the magnetic shielding characteristics in both configurations. Above full penetration of the cylinder, the presence of the superconductor is shown to affect the distribution of the three components of the flux density quite differently from each other. A 2D finite element model using an $\mathbf{A} - \phi$ formulation has been developed to model the axial configuration, using superconducting parameters ($J_c(\mathbf{B})$ and n) obtained from independent measurements in uniform field. The 2D modelling gives results that are in excellent agreement with experimental results. It has been employed to study the magnetic field and current density distributions inside the superconducting shield. The maximum field (at the centre of the emitting coil) that can be shielded with a superconducting tube, when it is subjected to the magnetic field of an emitting coil placed coaxially to the tube and at its centre, has been approximated analytically with a simple 1D model, and is remarkably good agreement with the 2D model as well as the experimental data. It predicts and quantifies the phenomenon of magnetic flux concentration that occurs between the emitting coil and the inner surface of the superconductor and which can be calculated analytically. In spite of its simplicity, this model can therefore be used to estimate at first magnetic shielding properties of various tubular screens in view of practical applications. Both 1D and 2D models were used to study the influence of the tube geometrical characteristics on the magnetic shielding properties.

Acknowledgements

We acknowledge P. Harmeling and J. Simon for technical help, as well as S. Kirsch and M. Philippe for fruitful discussions. We thank the *Communauté Française de Belgique* under reference ARC 11/16-03 for cryofluids and equipment grants.

References

[1] Pizzella V, Della Penna S, Del Gratta C and Luca Romani G 2001 *Supercond. Sci. Technol.* **14** R79

[2] Kamiya K, Warner B and DiPirro M 2001 *Cryogenics* **41** 401

[3] Holmes J J 2008 *Synth. Lect. Comput. Electromagn.* **3** 1

[4] Giunchi G, Bassani E, Cavallin T, Bancone N and Pavese F 2007 *Supercond. Sci. Technol.* **20** L39

[5] Hofman M B M et al. 2013 *Med. Phys.* **40** 012303

[6] P Arpaia, A Ballarino, G Giunchi and G Montenero 2014 *JINST* **9** P04020

[7] Willis J O, McHenry M E, Maley M P and Sheinberg H 1989 *IEEE Trans. Magn.* **25** 2502

[8] Pavese F 1998 *Handbook of Applied Superconductivity* (Bristol: Institute of Physics) p 1461

[9] Gozzelino L *et al* 2011 *J. Supercond. Novel Magn.* **24** 307

[10] Kumakura H *et al* 2003 *Physica C* **384** 283

[11] Soltanian S *et al* 2001 *Physica C* **361** 84

[12] Fagnard J-F, Elschner S, Bock J, Dirickx M, Vanderheyden B and Vanderbemden P 2010 *Supercond. Sci. Technol.* **23** 095012

[13] Rabbers J J, Oomen M P, Bassani E, Ripamonti G and Giunchi G 2010 *Supercond. Sci. Technol.* **23** 125003

[14] Fagnard J-F, Dirickx M, Ausloos M, Lousberg G, Vanderheyden B and Vanderbemden P 2009 *Supercond. Sci. Technol.* **22** 105002

[15] Kamiya K, Warner B A, Numazawa T 2004 *IEEE Trans. Magn*. **14** p 1042

[16] Denis S, Dusoulier L, Dirickx M, Vanderbemden P, Cloots R, Ausloos M and Vanderheyden B 2007 *Supercond. Sci. Technol.* **20** 192

[17] Frankel D 1979 *IEEE Trans. Magn.* **15** 1349

[18] Bhagwat K V and Chaddah P 1991 *Phys. Rev.* B **44** 6950

[19] Plechacek V, Hejtmanek J, Sedmidubsky D, Knizek K, Pollert E, Janu Z and Tichy R 1995 *IEEE Trans. Appl. Supercond.* **5** 528

[20] Sanchez A and Navau C *Phys. Rev. B* **64** 214506

[21] Kvitkovic J, Patil P, Pamidi S V. and Voccio J 2011 *IEEE Trans. Appl. Supercond.* **21** 1477

[22] Fagnard J-F, Vanderheyden B and Vanderbemden P 2012 *Superconductivity: Recent Developments and New Production Technologies* Miryala M (Hauppauge NY) Nova Science Publishers

[23] Navau C and Sanchez A *Phys. Rev. B* **64** 214507

[24] Gömöry F 2012 *Nature* **335** 1466

[25] http://www.can-superconductors.com/magnetic-shields.html

[26] Kim Y B, Hempstead C F and Strnad A R 1962 *Phys. Rev. Lett.* **9** 306-9

[27] Rhyner J 1993 *Physica C* **212** 292

[28] Caplin A D *et al* 1994 *Supercond. Sci. Technol.* **7** 412

[29] Campbell A 2011 *Supercond. Sci. Technol.* **24** 091001

[30] Brandt E H and Mikitik G P 2007 *Phys. Rev.* B **76** 064526

[31] Clem J R, Weigand M, Durrell J H and Campbell A M 2011 *Supercond. Sci. Technol.* **24** 062002

[32] Ruiz H S, Badia-Majos A and Lopez C 2011 *Supercond. Sci. Technol.* **24** 115005

[33] Henrotte F, Meys B, Hedia H, Dular P and Legros W 1999 *IEEE Trans. Magn.* **35** 1434

[34] Dular P and Geuzaine C 2006 *GetDP Reference Manual: The Documentation for GetDP, a General Environment for the Treatment of Discrete Problems* (http://www.geuz.org/getdp/)

[35] Brandt E H 1998 *Phys. Rev.* B **58** 6506

[36] Vanderbemden P, Destombes C, Cloots R and Ausloos M 1998 *Supercond. Sci. Technol.* **11** 94

[37] Müller K-H, Nikolo M and Driver R 1991 *Phys. Rev. B* **43** 7976